IET Generation, Transmission & Distribution

Research Article

IET Journals
The Institution of Engineering and Technology

Expansion planning for active distribution networks considering deployment of smart management technologies

ISSN 1751-8687
Received on 26th February 2018
Revised 06th August 2018
Accepted on 24th August 2018
doi: 10.1049/iet-gtd.2018.5882
www.ietdl.org

Changsen Feng[1], Weijia Liu[1], Fushuan Wen[1] ✉, Zhiyi Li[2], Mohammad Shahidehpour[2], Xinwei Shen[3]

[1]*School of Electrical Engineering, Zhejiang University, Hangzhou 310027, People's Republic of China*
[2]*Department of Electrical and Computer Engineering, Illinois Institute of Technology (IIT), Chicago 60605, USA*
[3]*Tsinghua-Berkeley Shenzhen Institute, Shenzhen 518055, People's Republic of China*
✉ *E-mail: fushuan.wen@gmail.com*

Abstract: In this study, a multi-stage long-term expansion planning model for an active distribution network (ADN) is presented, with the aim of minimising the investment and operation cost in a coordinated manner over an established horizon. The planning model optimises the following alternatives: upgrading the capacities of substations, reinforcing and/or constructing cable circuits, placing voltage regulators (VRs) and/or static VAR generators, and determining the connection points for distributed generators (DGs). The investment decisions are optimised over the entire planning horizon which can be further divided into multiple periods, and the operation strategies, e.g. active management of DG as well as ADN topology reconfiguration, are determined according to the profiles of representative scenarios. To relieve the computational burden, the original model is properly simplified as a mixed-integer quadratic constrained programming problem through linearisation and approximation techniques, and the solution optimality is guaranteed after invoking the off-the-shell solver. A 24-node test system is employed to validate the effectiveness of the proposed model.

Nomenclatures

Sets

Ω_t	set of periods
Ω_l	set of distribution lines
Ω_b	set of nodes
Ω_{bp}	set of transfer nodes
Ω_S	set of scenarios
Ω_{SR}	set of substation nodes
Ω_{LR}	set of candidate lines to be replaced
Ω_{LA}	set of candidate lines to be added
Ω_{VR}	set of candidate lines to build up VRs
Ω_{SVG}	set of static VAR generator (SVG) nodes
Ω_{DG}	set of candidate connection points for distributed generators (DGs)
Ψ_{SR}	set of alternatives for substations
Ψ_L	set of alternatives for conductors
Ψ_{VR}	set of alternatives for VRs

Parameters

$CINV$	investment cost, \$
$COPE$	operation cost, \$
CS_c	investment cost of type c reinforcement for the substation, \$
CL_l	investment cost of type l conductor, \$
CVR_d	investment cost of type d voltage regulator, \$
CSG	investment cost of SVG, \$/kVAR
$C_{s,t}^{\mathrm{DG}}$	cost for the curtailment of DG, \$/kW
$C_{s,t}^{\mathrm{loss}}$	cost for the network loss, \$/kW
Int	interest rate
τ_s	duration in scenario s, hour
Υ	number of blocks in the piecewise linearisation function
M	sufficiently large number
R_{ij}^l/X_{ij}^l	resistance/reactance of type l conductor of line ij
$\underline{V}/\bar{V}$	lower/upper limit for nodal voltage magnitude
$P_{i,s,t}^{\mathrm{DG,nom}}$	rated active power of the DG i in scenario s at period t
$Q_{\min}^{\mathrm{cap}}$	minimum capacity for the newly-built SVG
$S_{\mathrm{VRmax},d}$	thermal limit of the type d VR
$S_{\mathrm{DG},i}$	rating of the inverter of the DG i
$S_{\max,l}$	thermal limit of the type l conductor

Continuous variables

$r_{i,s,t}^{\mathrm{DG}}$	curtailed active power of DG at node i in scenario s at period t
$P_{i,s,t}^{\mathrm{SR}}/Q_{i,s,t}^{\mathrm{SR}}$	active/reactive power injection in substation i in scenario s at period t
$P_{ij,s,t}^l/Q_{ij,s,t}^l$	active/reactive power flow in line ij associated with conductor type l in scenario s at period t
$I_{ij,s,t}^l$	square of the current magnitude in line ij associated with conductor type l in scenario s at period t
$V_{i,s,t}$	square of the nodal voltage magnitude at node i in scenario s at period t
$Q_{i,s,t}^{\mathrm{CB}}$	charging power at node i in scenario s at period t
$SL_{ij,s,t}$	slack variable used in the calculation of the voltage drop of line ij in scenario s at period t

Binary variables

$\alpha_{ij,s,t}^+/\alpha_{ij,s,t}^-$	auxiliary variable indicating the direction of line ij in scenario s at period t
$x_{i,c,t}^{\mathrm{SR}}$	decision variable for reinforcement of the substation at bus i using type c substation at period t
$x_{ij,l,t}^{\mathrm{LR}}$	decision variable for reinforcement of line ij using type l conductor at period t
$x_{ij,l,t}^{\mathrm{LA}}$	decision variable for construction of line ij using type l conductor at period t
$x_{ij,d,t}^{\mathrm{VR}}$	decision variable for construction of type d VR in line ij at period t
$x_{i,t}^{\mathrm{SVG}}$	decision variable for construction of SVG at node i at period t
$x_{i,t}^{\mathrm{DG}}$	decision variable for construction of DG at bus i at period t
$\varepsilon_{i,t}$	decision variable that indicates whether transfer node i is used at period t

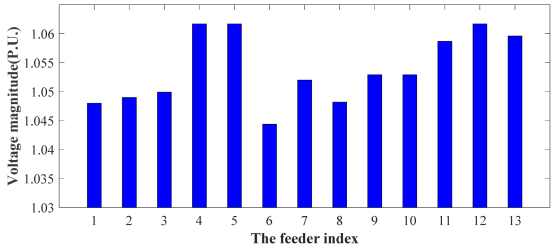

Fig. 1 *Voltage magnitude of the feeders*

$y^{l}_{ij,s,t}$ decision variable that indicates on–off status of line ij using type l conductor in scenario s at period t.

$\kappa^{in}_{ij,s,t}$ decision variable for existing line ij in scenario s at period t

1 Introduction

The goal of distribution network planning (DNP) is to determine the network expansion scheme at minimum investment and operation costs, aiming to serve the growing load demand and improve the power quality. Major options of DNP include constructing new lines, reinforcing substations, building up new distributed generators (DGs) and power electronic devices and others.

1.1 Motivation

The voltage rise is an urgent issue to address in some urban distribution systems in China. Fig. 1 shows the voltage magnitude at 10:00 PM of 8 February 2016 (a day of Chinese-New-Year holiday) in an actual 10 kV urban distribution power system in Zhejiang province, China. There are broadly two reasons that account for the voltage rise in urban distribution systems. One is the increasing penetration of DGs in modern distribution systems, which is also a major driving force for distribution network expansion/reinforcement and has been highlighted and addressed in many publications [1]. The other reason is that the underground power cables have been widely applied in distribution networks as a result of industrialisation and urbanisation in China. The capacitances of the underground cables may generate a large amount of reactive power and result in significant voltage rise issues, especially during the valley load period. Unfortunately, most businesses have the majority of their electricity usages between 8 AM and 6 PM while their weekend and night usages are typically lower. Hence, different from the existing publications that focus on VAR compensation and voltage drop, the voltage rise along with the role of reactive power should be better investigated in the expansion planning stage of a distribution network.

Power electronic devices, such as active power filters, static VAR compensators (SVCs) and static VAR generator (SVG), have been widely applied to improve power quality [1]. Among these techniques, the SVG is receiving increasing attentions from both academic and industrial communities due to its advantages such as continuous reactive power output, a wider range of regulation, and greater application flexibility. Hence, the investment and implementation of power electronic devices such as SVG should be considered as an alternative option in the DNP model.

With the development of real-time control techniques and communication systems, active network management (ANM) may better exploit DGs and other smart energy apparatuses to enhance the controllability and reliability of the distribution system concerned through certain schemes such as dynamic ratings, dynamic reconfiguration, and power factor control. Thus, ANM and other smart grid solutions should be incorporated into the DNP model as well.

A literature review of DNP and corresponding solution methods are given below.

1.2 Literature review

The DNP problem can be divided into two broad categories, i.e. static and multistage. In general, the static DNP problem is modelled in a single period while in the multistage model the investment decisions are made over successive planning periods [2]. Hence, in the multistage model, the investment decisions are made to accommodate the growing load demand and the future integration of DGs in the least cost way for the entire planning horizon. Accordingly, the traditional multistage DNP is typically modelled as a mixed-integer non-linear programming (MINLP) problem of which the objective usually consists of two parts: investment and operation costs. Tabares *et al.* [2] present a mixed-integer linear programming (MILP) model to solve the multistage long-term expansion planning problem whose objective function is defined as the minimisation of the investment and operation costs. Mohtashami *et al.* [3] present a multi-epoch DNP optimisation model in a distribution system with high penetration of DGs, and smart grid technologies are considered. Shen *et al.* [4] propose a co-optimisation method to solve the expansion planning problem of an active distribution network (ADN) with energy storage systems (ESSs) by minimising the long-term investment costs and the short-term operating costs. A bi-level model for ADN expansion planning considering renewable energy generation is proposed in [5], wherein the upper level addresses the investment decision-making problem while the lower one optimises the demand level according to the profiles of electricity prices. Mansor and Levi [6] provide a two-stage optimisation model for integrated planning of actual medium-voltage networks in the UK based on the utility planning concepts.

The investment cost mainly comprises construction cost and reinforcement cost. Correspondingly, alternative options for DNP include reinforcement and/or construction of lines, substations, and feeders [7], optimal siting and sizing of DG units [3, 8] and so on. Besides, more and more expansion alternatives, such as VRs and capacitor banks, are incorporated into the multistage DNP to mitigate the voltage deviation problem [9]. On the other hand, the operation cost includes the maintenance cost, energy loss, operation cost of substations [2], DG curtailment cost and load-shedding cost [3], costs of electricity procurement from the upstream power system and DGs [4], and reliability cost [10]. It should be mentioned that the reliability assessment is typically considered in the operation stage in some existing publications. The reliability indices are calculated to analyse the expansion planning candidates obtained from an investment cost minimisation model in [11], while Delgado *et al.* [12] provide an algebraic expression for reliability. In the model to be developed in this work, the characteristics of underground cables, utilisation of SVGs, and the implementation of smart grid technologies, e.g. ANM, are incorporated into the multistage DNP model with the network loss and DG curtailment cost being taken into account.

ANM is defined as a smart control strategy, e.g. adaptive power factor (APF) and active power curtailment (APC), which aims at maximising the utilisation of network assets and facilitating the integration of high penetration levels of DGs into the distribution network concerned [13]. Koutsoukis *et al.* [9] consider two categories of techniques for ANM: active power factor control and APC. Detailed formulations of various potential photovoltaic (PV) inverter control schemes for the DNP problem are presented in [13]. In [14], active management constraints for controllable components in ADN, e.g. DGs, controllable loads, and on load tap changers (OLTCs), are considered in the operation stage. Dzamarija and Keane [15] present the mathematical formulations of reactive power capabilities for the firm and non-firm wind generations, respectively.

The flexible topology is the key feature of the ADN through remote-control switches [4, 16], which can effectively reduce the network loss and minimise the energy shortage through distribution network reconfiguration (DNR). Cortes *et al.* [17] offer the optimal design of a microgrid topology in ADN following an iterative procedure, wherein graph partitioning, integer programming, and performance index are applied for the optimal design. Dias *et al.* [18] allow the closed-loop operation and minimises the number of the loops that ADN may present. Che *et al.* [19] solve the interconnection planning problem for a community of microgrids using a cut-set-based iterative method. Shu *et al.* [20] determine the topology of an ADN based on the raster map in geographic

information systems. Taylor and Hover [21] provide several convex models for the reconfiguration of the radial network.

As the power flow equations introduce quadratic inequalities that render most DNP problem non-convex, the DNP problem is typically modelled as a MINLP problem and solved by commercial solvers [9] or benders-decomposition-based algorithms [18]. Unfortunately, the above methods cannot guarantee to find global optimal solutions in a reasonable amount of time due to the significant computational complexity of the corresponding MINLP problems. Some heuristic algorithms are applied to solve the DNP problem, such as artificial bee colony algorithm [22] and simulated annealing algorithm [7]. In addition, the mix-integer convex model based on the conic quadratic format of the power flow is proposed in [8, 14]. However, the conditions for the exact conic relaxation is too strict for the DNP model as the direction of power flow can hardly be determined in advance [23]. In [4, 11, 12], a lossless DC power flow model is applied, which transformed the original DNP model into a MILP model. In our paper, some linearisation and approximation techniques are employed to transform the branch-flow-based DNP model into a mixed-integer quadratic constrained programming (MIQCP) problem which is tractable for most off-the-shell solvers.

1.3 Our contributions

From the literature review above, it seems clear that multiple planning alternatives with the consideration of the ANM and smart technologies in the solutions of the multistage long-term DNP problem has not been thoroughly examined. Different from many existing studies, our paper considers both conventional expansion options, such as upgrading the capacity of transformers and the circuits, as well as the smart grid technologies, i.e. ANM and DNR, and the utilisation of underground cables and SVGs. The model also takes into account the integration of DG units with a pre-specified capacity that are owned by third parties and determines their optimal connection points to the existing network to reduce the overall operation cost in the long run. The investment decisions of the multistage DNP are co-optimised with the optimal operation strategies of the multi-scenario in the proposed model. The main contributions are summarised in the following aspects:

i. To take into account the long-standing voltage rise and the widespread usage of underground cables in many urban distribution networks, we first present the fundamental models for underground cables and SVGs and then incorporated them into the alternative options.
ii. The new alternative option, i.e. choices of optimal DG connection points, together with smart technologies, i.e. ANM and DNR, are comprehensively integrated, which are likely to provide a more applicable and practical planning scheme.

The remaining of the paper is organised as follows. The model formulation is introduced in Section 2. The solution methodology is presented in Section 3. Case studies and numerical results are carried out in Section 4, followed by the conclusions together with future work in Section 5.

2 Model formulation

2.1 Objective function

The objective considers the total cost of investment and operation during the entire planning horizon. The first part is the net present value (NPV) of the investment cost while the second part corresponds to the costs associated with the DG curtailment cost and the network loss cost, which can be formulated as

$$\min \sum_{t \in \Omega_t} \frac{1}{(1+\mathrm{Int})^{t-1}} [\mathrm{CINV}_t + \mathrm{COPE}_t] \tag{1}$$

where

$$\mathrm{CINV}_t = IC_{\mathrm{SR},t} + IC_{\mathrm{LR},t} + IC_{\mathrm{LA},t} + IC_{\mathrm{VR},t} + IC_{\mathrm{SVG},t} \tag{2}$$

$$IC_{\mathrm{SR},t} = \sum_{i \in \Omega_{\mathrm{SR}}} \sum_{c \in \Psi_{\mathrm{SR}}} CS_c x^{\mathrm{SR}}_{i,c,t} \tag{3}$$

$$IC_{\mathrm{LR},t} = \sum_{ij \in \Omega_{\mathrm{LR}}} \sum_{l \in \Psi_L} CL_l x^{\mathrm{LR}}_{ij,l,t} \tag{4}$$

$$IC_{\mathrm{LA},t} = \sum_{ij \in \Omega_{\mathrm{LA}}} \sum_{l \in \Psi_L} CL_l x^{\mathrm{LA}}_{ij,l,t} \tag{5}$$

$$IC_{\mathrm{VR},t} = \sum_{ij \in \Omega_{\mathrm{VR}}} \sum_{d \in \Psi_{\mathrm{VR}}} CVR_d x^{\mathrm{VR}}_{ij,d,t} \tag{6}$$

$$IC_{\mathrm{SVG},t} = \sum_{i \in \Omega_{\mathrm{SVG}}} Q^{cap}_{i,t} \times CSG \tag{7}$$

$$\mathrm{COPE}_t = \sum_{s \in \Omega_S} \tau_s \left(\sum_{i \in \Omega_{\mathrm{DG}}} C^{\mathrm{DG}}_{s,t} r^{\mathrm{DG}}_{i,s,t} + \sum_{ij \in \Omega_l} C^{\mathrm{loss}}_{s,t} I_{ij,s,t} R_{ij,s,t} \right) \tag{8}$$

$$\begin{aligned} &\sum_{k:(ki) \in \Omega_l} \sum_{l \in \Psi_L} \left(P^l_{ki,s,t} + P^{\mathrm{in}}_{ki,s,t} - I^l_{ki,s,t} R^l_{ki} \right) + \sum_{i \in \Omega_{\mathrm{DG}}} P^{\mathrm{DG}}_{i,s,t} \\ &- \sum_{j:(ij) \in \Omega_l} \sum_{l \in \Psi_L} (P^l_{ij,s,t} + P^{\mathrm{in}}_{ij,s,t}) - \sum_{i \in \Omega_D} P^D_{i,s,t} = 0 \end{aligned} \tag{9}$$

$$\begin{aligned} &\sum_{k:(ki) \in \Omega_l} \sum_{l \in \Psi_L} \left(Q^l_{ki,s,t} + Q^{\mathrm{in}}_{ki,s,t} - I^l_{ki,s,t} X^l_{ki} \right) + \sum_{i \in \Omega_{\mathrm{SVG}}} Q^{\mathrm{SVG}}_{i,s,t} \\ &+ \sum_{i \in \Omega_b} Q^{\mathrm{CB}}_{i,s,t} - \sum_{j:(ij) \in \Omega_l} \sum_{l \in \Psi_L} (Q^l_{ij,s,t} + Q^{\mathrm{in}}_{ij,s,t}) + \sum_{i \in \Omega_{\mathrm{DG}}} Q^{\mathrm{DG}}_{i,s,t} = 0 \end{aligned} \tag{10}$$

Note that the construction cost for SVG here is proportional to the capacity of SVG, and the installed cost per SVG unit is assumed as a constant [3].

To be more specific, the DGs considered in our model are referred to wind farms deployed at the distribution level. They are owned by the third parties (e.g. independent wind power producers), which is a common practice in Europe and the US (see [9, 24, 25]). We further assume that the electric utility company and those DGs owners have a contractual agreement usually called *take-or-pay* contract [24, 25]. In this contract, the electric utility company accepts all available electricity generated from wind farms at a fixed price which is typically lower than the retail electricity price. Similar to [6], the production costs of electricity from substations and DGs are not taken into consideration based on the utility planning concepts.

2.2 ADN operation constraints

The grid static security constraints are composed of three aspects: the power balance, limits on branch flows and nodal voltage magnitudes, and topology logic constraints in ADN operation.

2.2.1 Power balance and thermal limit: Different from the overhead distribution lines, the capacitance of the underground cable is generally very large and should not be neglected. Here the underground cable is modelled with the standard π single-line model, with series impedance Z_{ij} and total charging susceptance Y_{ij}, as shown in Fig. 2. For any $i \in \Omega_b \setminus \Omega_{\mathrm{SR}}$, at any $s \in \Omega_S$, and at any $t \in \Omega_t$, we have

$$P_{ij,s,t} = \sum_{l \in \Psi_L} P^l_{ij,s,t} \quad \forall ij \in \Omega_l \tag{11}$$

$$Q_{ij,s,t} = \sum_{l \in \Psi_L} Q^l_{ij,s,t} \quad \forall ij \in \Omega_l \tag{12}$$

$$I_{ij,s,t} = \sum_{l \in \Psi_L} I^l_{ij,s,t} \quad \forall ij \in \Omega_l \tag{13}$$

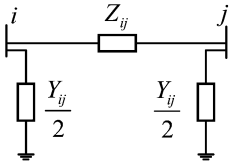

Fig. 2 *Single-line model for the underground cable*

$$Q_{i,s,t}^{\mathrm{CB}} = 1/2 \sum_{l \in \Psi_L} \left(\sum_{ij \in \Omega_l} V_{i,s,t} Y_{ij}^{l} y_{ij,s,t}^{l} + \sum_{ki \in \Omega_l} V_{i,s,t} Y_{ki}^{l} y_{ki,s,t}^{l} \right) \quad (14)$$

$$\left(P_{ij,s,t}^{\mathrm{in}}\right)^2 + \left(Q_{ij,s,t}^{\mathrm{in}}\right)^2 \le S_{\max}^2 \kappa_{ij,s,t}^{\mathrm{in}} \quad \forall ij \in \Omega_{\mathrm{LR}} \quad (15)$$

$$\left(P_{ij,s,t}^{l}\right)^2 + \left(Q_{ij,s,t}^{l}\right)^2 \le \sum_{l \in \Psi_L} S_{\max,l}^2 y_{ij,s,t}^{l} \quad \forall ij \in \Omega_l \quad (16)$$

Equations (9) and (10) shown at the bottom represent the active/reactive power balance for each node. The total active and reactive power, and the square of the total current flow magnitude are calculated using (11)–(13). The charging power of the susceptance of the cable at node i, denoted as $Q_{i,s,t}^{\mathrm{CB}}$, can be calculated using (14). Constraints (15) and (16) are the thermal limits of the circuit according to the planning period and the corresponding type of the conductor, respectively.

The distribution transformers should upgrade their capacities in accordance with the demand growth. For any $i \in \Omega_{\mathrm{SR}}$, in any $s \in \Omega_S$ at any $t \in \Omega_t$, we have

$$\left(P_{i,s,t}^{\mathrm{SR}}\right)^2 + \left(Q_{i,s,t}^{\mathrm{SR}}\right)^2 \le S_{\mathrm{SRmax}}^2 + S_{\mathrm{SRmax},c}^2 \sum_{h=1}^{t} x_{i,c,h}^{\mathrm{SR}} \forall c \in \Psi_{\mathrm{SR}} \quad (17)$$

Constraint (17) imposes the limit on the capacities of the transformers.

2.2.2 Voltage magnitude limit: In fact, the nodal voltage magnitude is regulated into the statutory ranges to maintain the power delivery. For any $ij \in \Omega_l \setminus \Omega_{\mathrm{VR}}$, in any $s \in \Omega_S$ at any $t \in \Omega_t$ we obtain

$$V_{j,s,t} = V_{i,s,t} - \sum_{l \in \Psi_L} [2(P_{ij,s,t}^{l} R_{ij}^{l} + Q_{ij,s,t}^{l} X_{ij}^{l}) + ||Z_{ij}^{l}||_2^2 IL_{ij,s,t}] + SL_{ij,s,t} \quad (18)$$

$$V_{i,s,t} I_{i,s,t} = P_{ij,s,t}^2 + Q_{ij,s,t}^2 \quad (19)$$

$$\underline{V}^2 \le V_{j,s,t} \le \bar{V}^2 \quad (20)$$

$$\left|SL_{ij,s,t}\right| \le M(1 - \alpha_{ij,s,t}^{+} - \alpha_{ij,s,t}^{-}) \quad (21)$$

Equation (18) shown at the bottom calculates the voltage drop in the circuit. Equation (19) establishes the relationship between the square of the current flow magnitude, the square of nodal voltage magnitude, and the power flow. Constraint (20) represents limits on the nodal voltage magnitude. Constraint (21) establishes the relationship between the slack variable of a circuit and its operation stage.

2.2.3 Topology logic constraints in ADN operation: As most distribution systems are meshed in design and operated radially as a tradeoff between the investment cost of protection system and reliability, here the radiality is considered as a set of constraints and stated for any $t \in \Omega_t$ in any $s \in \Omega_S$ as

$$\kappa_{ij,s,t} + \sum_{l \in \Psi_L} y_{ij,s,t}^{l} = \alpha_{ij,s,t}^{+} + \alpha_{ij,s,t}^{-} \quad \forall ij \in \Omega_{\mathrm{LR}} \quad (22)$$

$$\sum_{l \in \Psi_L} y_{ij,s,t}^{l} = \alpha_{ij,s,t}^{+} + \alpha_{ij,s,t}^{-} \quad \forall ij \in \Omega_{\mathrm{LA}} \quad (23)$$

$$\alpha_{ij,s,t}^{+} + \alpha_{ij,s,t}^{-} \le 1 \quad \forall ij \in \Omega_l \quad (24)$$

$$\sum_{ij \in \Omega_l} (\alpha_{ij,s,t}^{+} + \alpha_{ij,s,t}^{-}) = |\Omega_b| - |\Omega_{\mathrm{SR}}| - \sum_{i \in \Omega_{bp}} (1 - \varepsilon_{i,t}) \quad (25)$$

$$\sum_{ij \in \Omega_l} \alpha_{ij,s,t}^{+} + \sum \alpha_{ki,s,t}^{-} \ge 2\varepsilon_{i,t} \quad (26)$$

$$\alpha_{ij,s,t}^{+} + \alpha_{ij,s,t}^{-} \le \varepsilon_{i,t} \quad \forall i \in \Omega_{bp} \quad (27)$$

$$\alpha_{ji,s,t}^{+} + \alpha_{ji,s,t}^{-} \le \varepsilon_{i,t} \quad \forall i \in \Omega_{bp} \quad (28)$$

Constraints (22)–(28) ensure the radial operation of the system and are the work done in [26].

As DGs can feed some loads independently, in some cases (22)–(28) may lead to undesirable solutions where certain DGs operate in the islanding mode. Thus, additional constraints should be added to ensure that a DG is not isolated from the substation. Here, the virtual loads which can only be fed by the substation are added at each node associated with the DG and stated for any $t \in \Omega_t$ in any $s \in \Omega_S$ as

$$\sum_{ij \in \Omega_l} \rho_{ij,s,t} - \sum_{ki \in \Omega_l} \rho_{ki,s,t} = \delta_{i,s,t} \quad \forall i \in \Omega_b \quad (29)$$

$$\delta_{i,s,t} = \sum_{h=1}^{t} x_{i,t}^{\mathrm{DG}}, \quad \forall i \in \Omega_{\mathrm{DG}} \quad (30)$$

$$\delta_{i,s,t} = 0 \quad \forall i \notin \Omega_{\mathrm{DG}} \cup \Omega_{\mathrm{SR}} \quad (31)$$

$$\left|\rho_{ij,s,t}\right| \le M(\alpha_{ij,s,t}^{+} + \alpha_{ij,s,t}^{-}) \quad (32)$$

where $\delta_{i,s,t}$ represents the virtual load at bus i in scenario s at period t, $\rho_{ij,s,t}$ is the virtual power flow associated with branch ij in scenario s at period t.

2.3 Smart component modelling

2.3.1 Voltage regulator (VR) modelling: The VR is modelled with a cable in series with an ideal transformer. The transformer with a tap ratio aR, is located at the to-end of the branch, as shown in Fig. 3. Here it's assumed that all the VRs have the same regulator range, as well as the same tap step. Considering the long-term property of the proposed model, the tap position of VRs is further assumed as a continuous variable. The VR model is stated for any $ij \in \Omega_{\mathrm{VR}}$, in any $s \in \Omega_S$, at any $t \in \Omega_t$ as follows:

$$(1 - a_R)^2 v_{j,s,t} \le V_{j,s,t} \le (1 + a_R)^2 v_{j,s,t} \quad (33)$$

$$\left|v_{j,s,t} - V_{j,s,t}\right| \le \left(\bar{V}^2 - \underline{V}^2\right) \sum_{l \in \Psi_L} y_{ij,s,t}^{l} \quad (34)$$

$$\left|v_{j,s,t} - V_{j,s,t}\right| \le \left(\bar{V}^2 - \underline{V}^2\right) \sum_{d \in \Psi_{\mathrm{VR}}} \sum_{h=1} x_{ij,d,t}^{\mathrm{VR}} \quad (35)$$

$$P_{ij,s,t}^2 + Q_{ij,s,t}^2 \le M\left(1 - \sum_{d \in \Psi_{\mathrm{VR}}} \sum_{h=1} x_{ij,d,t}^{\mathrm{VR}}\right) + \sum_{d \in \Psi_{\mathrm{VR}}} S_{\mathrm{VRmax},d}^2 \sum_{h=1} x_{ij,d,h}^{\mathrm{VR}} \quad (36)$$

The voltage magnitude $v_{j,s,t}$ can be calculated using (18). The constraint (36) denotes the thermal limit of the VRs.

2.3.2 SVG modelling: The SVG functions as a shunt-connected static synchronous voltage source whose capacitive or inductive

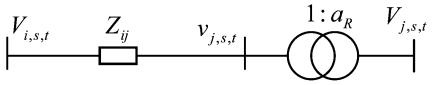

Fig. 3 *Model for VR*

output current can be controlled independently of the AC system voltage [1]. The SVG volt-ampere characteristics approach rectangular and thus have wider ranges compared with SVC inverse triangular operational characteristics. The maximum voltage and current are constrained by the SVG capacity. Considering the long-term property of the proposed model and neglecting the transient process, the operational and constructional constraints for SVGs are formulated for any $i \in \Omega_{\mathrm{SVG}}$, at any $t \in \Omega_t$ as follows:

$$-Q_{i,t}^{\mathrm{cap}} \le Q_{i,s,t}^{\mathrm{SVG}} \le Q_{i,t}^{\mathrm{cap}} \quad \forall s \in \Omega_S \tag{37}$$

$$Q_{i,t}^{\mathrm{cap}} \ge Q_{\min}^{\mathrm{cap}} x_{i,t}^{\mathrm{SVG}} \tag{38}$$

$$Q_{i,t}^{\mathrm{cap}} \le M x_{i,t}^{\mathrm{SVG}} \tag{39}$$

The constraint (37) is the maximum/minimum output power limit for the SVG in every scenario. Constraints (38) and (39) impose the minimum capacity limit on the newly-built SVG.

2.3.3 Optimal connection points and ANM for DG: It is assumed that each DG, which is referred to a wind farm deployed at the distribution network level in our model, will be connected to one of the multiple candidate connection points at period t^*. The constraints are stated for any $i \in \Omega_{\mathrm{DG}}$, at any $t \in \Omega_t$ as

$$0 \le P_{i,s,t}^{\mathrm{DG}} \le P_{i,s,t}^{\mathrm{DG,nom}} \sum_{h=1}^{t} x_{i,t}^{\mathrm{DG}} \tag{40}$$

$$\sum_{t \in \Omega_t} \sum_{i \in \Omega_{\mathrm{DG}}\{j\}} x_{i,t}^{\mathrm{DG}} = 1, \text{ and } \sum_{i \in \Omega_{\mathrm{DG}}\{j\}} x_{i,t^*}^{\mathrm{DG}} = 1 \tag{41}$$

where $\Omega_{\mathrm{DG}}\{j\}$ denotes the set of candidate entry nodes for the jth DG installation. Constraint (40) imposes the limit on the DG output power. Constraint (41) represents that only one DG unit can be applied at period t^* among the corresponding candidate nodes.

Here, it is assumed that the distribution network operator purchases all the available power of DGs at fixed prices through *take-or-pay* contracts. Thus, the operator is capable of implementing the ANM techniques. More specifically, the operator could adjust DGs' power factors or curtail the active power generations of DGs to balance the power in each time slot (e.g. hour) in the distribution system concerned. Implementations of APF control require complex control techniques and the actions of related smart devices. As the proposed technique is considered at the expansion planning stage, it is assumed that the smart components will respond immediately to actions and thus are operated in a steady state in each planning period [9]. With the use of APF control technology, the DGs can flexibly operate at leading, unity or lagging power factors. In practice, the power factors of DGs will be required to operate within a certain range considering the harmonic distortions. Assuming $cos(\theta)$ is the power factor limit, the reactive power injection is described for any DG i, in any $s \in \Omega_S$, at any $t \in \Omega_t$ as

$$-P_{i,s,t}^{\mathrm{DG,nom}} \tan(\arccos(\theta)) \le Q_{i,s,t}^{\mathrm{DG}} \le \tan(\arccos(\theta)) P_{i,s,t}^{\mathrm{DG,nom}} \tag{42}$$

The reactive power for the inverter-interfaced DG is also be jointly constrained by the active power of the DG and the inverter rating, as described below:

$$\left(Q_{i,s,t}^{\mathrm{DG}}\right)^2 + \left(P_{i,s,t}^{\mathrm{DG}}\right)^2 \le S_{\mathrm{DG},i}^2 \tag{43}$$

In addition to APF, the APC technique is commonly applied [13–15] to alleviate the voltage rise in ADN. Here, the APC is formulated by adding a virtual positive demand at each DG node, stated for any DG i, in any $s \in \Omega_S$, at any $t \in \Omega_t$ as

$$P_{i,s,t}^{\mathrm{DG}} = P_{i,s,t}^{\mathrm{DG,nom}} - r_{i,s,t}^{\mathrm{DG}} \tag{44}$$

$$0 \le r_{i,s,t}^{\mathrm{DG}} \le \mu^{\mathrm{curt}} P_{i,s,t}^{\mathrm{DG,nom}} \tag{45}$$

$$\left|Q_{i,s,t}^{\mathrm{DG}}\right| \le P_{i,s,t}^{\mathrm{DG}} \tan(\arccos(\theta)) \tag{46}$$

Note that constraint (45) imposes the upper and lower limits on the curtailment of DGs.

2.4 Construction and operation logic constraints

$$\sum_{t \in \Omega_t} \sum_{c \in \Psi_{\mathrm{SR}}} x_{i,c,t}^{\mathrm{SR}} \le 1 \quad \forall i \in \Omega_{\mathrm{SR}} \tag{47}$$

$$\sum_{t \in \Omega_t} \sum_{l \in \Psi_L} x_{ij,l,t}^{\mathrm{LR}} \le 1 \quad \forall ij \in \Omega_{\mathrm{LR}} \tag{48}$$

$$\sum_{t \in \Omega_t} \sum_{l \in \Psi_L} x_{ij,l,t}^{\mathrm{LA}} \le 1 \quad \forall ij \in \Omega_{\mathrm{LA}} \tag{49}$$

$$\sum_{t \in \Omega_t} \sum_{d \in \Psi_{\mathrm{VR}}} x_{ij,d,t}^{\mathrm{VR}} \le 1 \quad \forall ij \in \Omega_{\mathrm{VR}} \cap \Omega_{\mathrm{LA}} \tag{50}$$

$$y_{ij,s,t}^{l} \le \sum_{h=1}^{t} x_{ij,l,t}^{\mathrm{LA}} \quad \forall ij \in \Omega_{\mathrm{LA}} \forall s \in \Omega_S \tag{51}$$

$$y_{ij,s,t}^{l} \le \sum_{h=1}^{t} x_{ij,l,t}^{\mathrm{LR}} \quad \forall ij \in \Omega_{\mathrm{LR}} \forall s \in \Omega_S \tag{52}$$

$$\kappa_{ij,s,t} = 1 - \sum_{l \in \Psi_L} \sum_{h=1}^{t} x_{ij,l,t}^{\mathrm{LR}} \quad \forall ij \in \Omega_{\mathrm{LR}}\ \forall s \in \Omega_S \tag{53}$$

$$\sum_{h=1}^{t} x_{ij,d,t}^{\mathrm{VR}} \le \sum_{h=1}^{t} x_{ij,l,t}^{\mathrm{LA}} \quad \forall ij \in \Omega_{\mathrm{VR}} \cap \Omega_{\mathrm{LA}} \tag{54}$$

Constraint (47) shows that the substation transformers can be reinforced once during the planning horizon. Besides, only one expansion option of the circuits can be chosen for one line, represented by constraints (48) and (49). Constraint (50) shows that no more than one VR can be allocated at each node. Constraints (51)–(53) describe that the candidate lines may only be used once the corresponding investment cost is made, which excludes the initial branch for replacement. Constraint (54) represents that the VRs can be allocated after the construction of the corresponding circuit. Note that the SVGs can be reinforced in every period and hence there are no such constraints for the SVGs.

3 Solution methodology

The power flow equations introduce quadratic inequalities related to voltage magnitudes and angles that render most optimisation problems over power networks non-convex and hence hard to solve. In this section, the non-linear terms in (14) and (19) are linearised to get a tractable MIQCP model for the DNP problem.

3.1 Linearisation of (14)

In this part, (14) is transformed into a big-M disjunctive constraint based on the Fortuny-Amat transformation. For any $ij \in \Omega_l$, in any $s \in \Omega_S$, at any $t \in \Omega_t$, the bilinear term in (14) $V_{i,s,t} Y_{ij}^{l} y_{ij,s,t}^{l}$ is linearised as

$$\begin{cases} -My^l_{ij,s,t} \le \omega^l_{ij,s,t} \le My^l_{ij,s,t} \\ V_{i,s,t}Y^l_{ij} - M(1-y^l_{ij,s,t}) \le \omega^l_{ij,s,t} \le V_{i,s,t}Y^l_{ij} + M(1-y^l_{ij,s,t}) \end{cases} \quad (55)$$

3.2 Linearisation of (19)

The left-hand term of (19) is a bilinear term which is intractable for off-the-shell solvers. Here, the estimated value for the nodal voltage magnitude is used to approximate the product $V_{i,s,t}I_{i,s,t}$ and stated as follows:

$$V_{i,s,t}I_{i,s,t} \simeq \hat{V}_{i,s,t}I_{i,s,t} \quad (56)$$

So far, constraint (19) is still not a standard convex set which is usually intractable for convex techniques. Thus, the right-hand term of (19) should be further approximated by the following linear expression [27]:

$$P^2_{ij,s,t} + Q^2_{ij,s,t} = \sum_{\gamma=1} m^{P,\gamma}_{ij,s,t}\Delta^{P,r}_{ij,s,t} + m^{Q,\gamma}_{ij,s,t}\Delta^{Q,\gamma}_{ij,s,t} \quad (57)$$

$$P_{ij,s,t} = P^+_{ij,s,t} - P^-_{ij,s,t} \quad (58)$$

$$Q_{ij,s,t} = Q^+_{ij,s,t} - Q^-_{ij,s,t} \quad (59)$$

$$P^+_{ij,s,t} + P^-_{ij,s,t} = \sum_{\gamma=1}^{\Upsilon} \Delta^{P,r}_{ij,s,t} \quad (60)$$

$$Q^+_{ij,s,t} + Q^-_{ij,s,t} = \sum_{\gamma=1}^{\Upsilon} \Delta^{Q,r}_{ij,s,t} \quad (61)$$

$$0 \le \Delta^{P,r}_{ij,s,t} \le P^{\max}_{ij,s,t}/\Upsilon \quad (62)$$

$$0 \le \Delta^{Q,r}_{ij,s,t} \le Q^{\max}_{ij,s,t}/\Upsilon \quad (63)$$

The two terms on the right-hand side of (57) are the linear approximation of $P^2_{ij,s,t}$ and $Q^2_{ij,s,t}$, respectively. $P^+_{ij,s,t}$ and $P^-_{ij,s,t}$ are the non-negative auxiliary variables to attain $P_{ij,s,t}$, whereas $Q^+_{ij,s,t}$ and $Q^-_{ij,s,t}$ are the non-negative auxiliary variables to attain $Q_{ij,s,t}$, respectively. Equations (60) and (61) describe the values of $|P_{ij,s,t}|$ and $|Q_{ij,s,t}|$, which can be calculated using the sum of the values in each block of the discretisation $\Delta^{P,r}_{ij,s,t}$ and $\Delta^{Q,r}_{ij,s,t}$, respectively. Constraints (62) and (63) impose the upper/lower limits on the discretisation variables $\Delta^{P,r}_{ij,s,t}$ and $\Delta^{Q,r}_{ij,s,t}$ in each block, respectively. The values of parameters in the discretisation, namely $m^{P,\gamma}_{ij,s,t}$ and $m^{Q,\gamma}_{ij,s,t}$, can be calculated through the following equations, respectively,

$$m^{P,\gamma}_{ij,s,t} = (2\gamma-1)P^{\max}_{ij,s,t}/\Upsilon \quad \gamma = 1,\ldots,\Upsilon \quad (64)$$

$$m^{Q,\gamma}_{ij,s,t} = (2\gamma-1)Q^{\max}_{ij,s,t}/\Upsilon \quad \gamma = 1,\ldots,\Upsilon \quad (65)$$

Accordingly, the original model is transformed into a MIQCP problem, stated as

$$\begin{cases} \min \quad (1) \\ \text{s.t.} \quad (9)-(13),(15)-(18),(20)-(65) \end{cases} \quad (66)$$

4 Case studies

In this section, a modified 24-bus distribution system is employed to validate the proposed model and solution methodology. The numerical experiments are conducted in MATLAB R2014a on a personal computer with an Intel Core (i5-4590, 3.30 GHz) and 8 GB random access memory. SCIP 3.2 [28] is invoked to solve the MIQCP.

4.1 Simulation data

The test system operates at a nominal voltage of 13.8 kV, consisting of 24 nodes and 34 branches. The initial topology of the ADN is presented in Fig. 4 [2], where the dashed lines represent the candidate lines for expansion while the solid lines are the installed circuits for replacement. For simplicity, the candidate lines for the allocation of VRs include lines 21-1, 21-2, 22-6 and 22-8. Here, it is assumed that SVGs can be installed at every node and reinforced at any period. The minimum capacity for the newly-constructed SVGs is 50 kVAR. CSG is set as \$80/kW, which is adapted from [3]. The annual discount rate of interest, Int, is 2.25%. μ^{curt} is set as 40%. In our case studies, the substation transformer operates with the leading power factor staying within an interval [0.85 0.95]. The expansion alternatives are listed in Tables 1–3.

It is assumed that the electricity price of DG and the electricity price in the upstream power system are, respectively, 30 and \$40/MWh in the *take-or-pay* contracts. The retail price for the consumers is assumed as \$50/MWh. Using these electricity prices, we give an estimation on the NPV and IRR of our model in different cases. A total planning horizon of 21 years is adopted in these case studies and is further divided into three periods (each representing 7 years).

Two representative scenarios are used to simulate the load and DGs' generation profile in each planning period. Specifically, we assume the low-level DG generation is 60% of the high-level DG generation. The pertinent data are available at http://motor.ece.iit.edu/data/EPData.xls. Distribution networks should be planned so as to accommodate the maximum stress scenarios during the planning period. Here, we define the maximum stress scenarios as

Scenario 1: maximum load/low-level DG power generation.
Scenario 2: minimum load/high-level DG power generation.

It is assumed that the DGs are owned by third parties and the new DGs to be connected are detailed as follows:

- DG 1 at bus 7 or 8: 5 MW at the beginning of the first period.
- DG 2 at bus 14 or 1: 5.5 MW at the beginning of the second period.
- DG 3 at bus 23: 6 MW at the beginning of the third period.
- DG 4 at bus 24: 6 MW at the beginning of the third period.

Five different cases are conducted to verify the proposed model. The case setups, the number of variables and constraints, together with the corresponding solution time are listed in Table 4.

4.2 Numerical results and analysis

In Figs. 4 and 5, continuous lines denote the lines built; ⊛ represents the VR; ⊣⊢ represents the allocation of an SVG; ⊡ is the substation, respectively. Table 5 presents an economic analysis of the five cases.

i. *Case 1:* The solution obtained in case 1 has an objective value of US\$ 1,367,100 and the case is solved in 50.1 min. In period 1, circuits 1-9, 9-4, 7-23 and 23-10 were built with the conductor type 1 while circuit 21-1 was reinforced by conductor type 2. Meanwhile, a VR was allocated to circuit 21-2 while the SVG with a capacity of 700 kVAR was allocated at node 21 to absorb the surplus of the reactive power from the upstream power system. In period 2, circuits 1-14, 2-12, 3-16, 3-23, 7-11, 6-13 and 17-15 were built with conductor type 1 and circuits 21-2, 2-3 and 22-17 were constructed with conductor type 2. Besides, the substation 21 was upgraded by 12 MWA while the SVGs with the capacity of 500 and 400 kVAR were installed at nodes 21 and 22, respectively. In period 3, circuits 14-18, 5-24, 24-20, and 15-19 were built with conductor type 1. Note that load at node 10 were transferred to substation 22 through the construction of circuit 7-23 in period 1. However, nodes 10 and 23 were

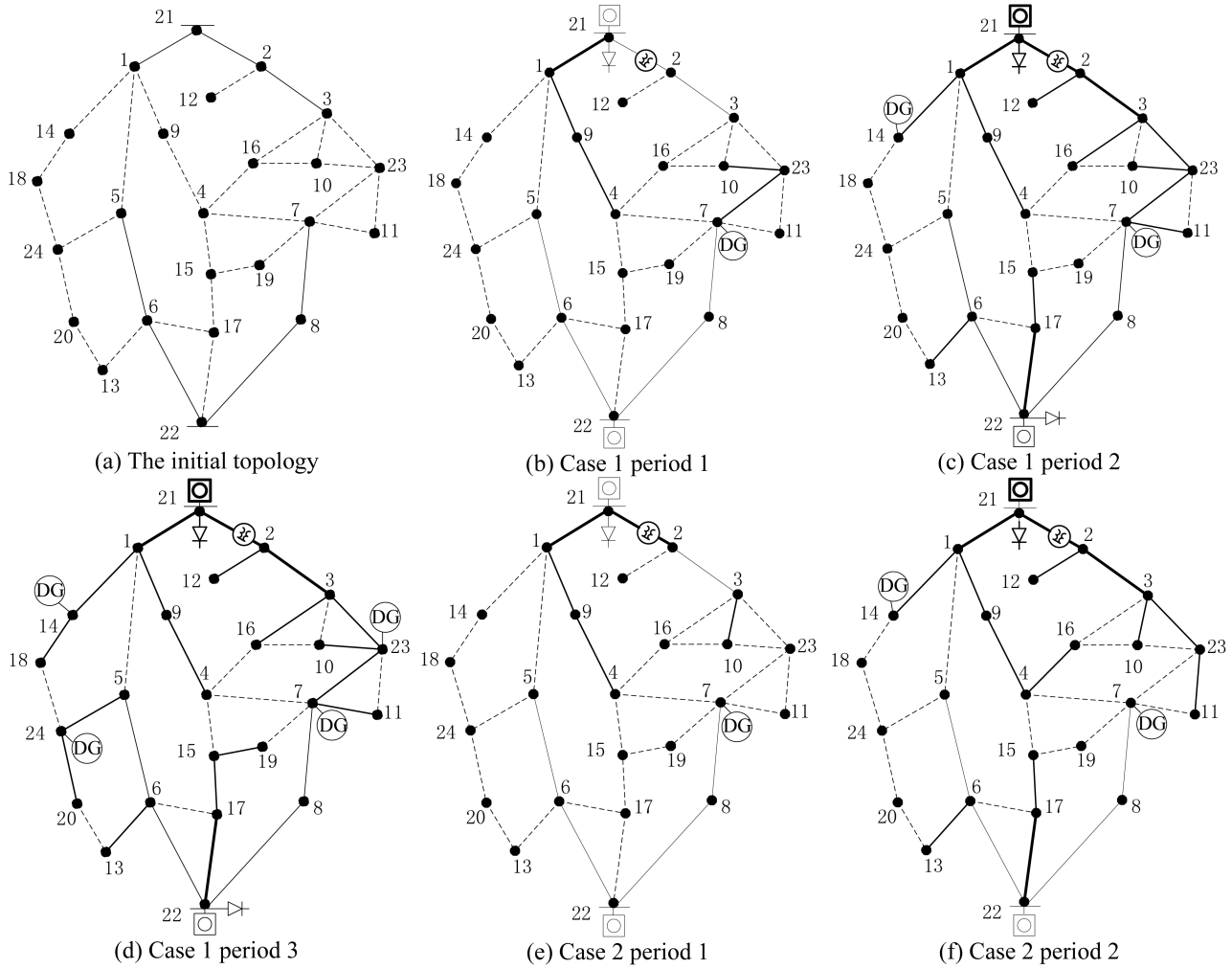

Fig. 4 *Topologies for the initial 24-node distribution system and cases 1 and 2*
(a) Initial topology, ***(b)*** Case 1 period 1, ***(c)*** Case 1 period 2, ***(d)*** Case 1 period 3, ***(e)*** Case 2 period 1, ***(f)*** Case 2 period 2

Table 1 Substation data

Type	Capacity, MVA	Cost, 10^3
1	12	100
2	20	300

Table 2 Conductor data

Type	Z, Ω/km	C, μF/km	Ampacity, A	Cost, 10^3/km
1	0.325 + j0.0907	0.43	270	25
2	0.102 + j0.0812	0.60	515	35

Table 3 VR data

Type	Capacity, MVA	Cost, 10^3
1	6	70
2	12	85

transferred to substation 21 through opening circuit 7-23 in periods 2 and 3. This is mainly because load at node 10 could be supplied by substation 22 in period 1 and thereby the construction of circuit 3-27 was postponed until period 2 for investment cost savings. In addition, loads at the nodes 7 and 11 were supplied by the DG at node 7 in both the scenarios 1 and 2 of periods 2 and 3 so as to avoid the DG curtailment. Note that due to the reconfigurations in the different planning periods and scenarios, the system topology for the two scenarios changes to minimise investment and operational costs. The total cost in case 1 is the lowest while the NPV and IRR are the highest among the five cases, which shows that our model guarantees an economic planning scheme.

ii. *Case 2:* The solution obtained in case 2 has an objective value of $ 1,440,100 and the case is solved in 40.3 min. In period 1, circuits 1-9, 9-4, and 3-10 were built with the conductor type 1 while circuits 21-1 and 21-2 were reinforced by the conductor type 2. Meanwhile, a VR was allocated to circuit 21-2 while the SVG with a capacity of 1000 kVAR was allocated at node 21 to absorb the surplus of reactive power from the upstream power system. In period 2, circuits 1-14, 2-12, 3-23, 23-11, 6-13 and 17-15 were built with the conductor type 1 while circuits 2-3 and 22-17 were constructed with the conductor type 2. Besides, the substation 21 was upgraded by 12 MWA while the SVG at node 21 was reinforced with a capacity of 1300 kVAR. In period 3, loads at nodes 23 and 11 were fed by substation 21 and the DG at node 23 in both scenarios. Besides, the SVG with a capacity of 300 kVAR was installed at substation 22 in period 3.

The total cost of case 2 is $73,000 (5.07%) higher than that of case 1. In particular, due to the absence of reconfiguration in the operation stage, load at 10 was supplied by substation 21, which results in the reinforcement of circuit 21-2 in period 1. Compared with case 1, the SVGs with larger capacities were installed in case 2 to mitigate the voltage rise which also incurs more investment. This can be explained by the impacts of the flexible topology in case 1. Specifically, the reconfiguration in case 1 offers the possibility of power flow control by optimally transferring loads and DGs' outputs.

iii. *Case 3:* The solution obtained in case 3 has an objective value of US$1,488,200 and the case is solved in 66.7 min. In this case, it is assumed that DGs in periods 1 and 2 were connected to nodes 8 and 1, respectively. The model in case 3 provides

the same solutions as case 2 in periods 1 and 2, except the sizing the SVG. In period 3, circuit 7-23 was built with the conductor type 1. In the operating stage, the circuit 3-23 was open in the scenario 1 so that the loads at nodes 10 and 23 were supplied by the DGs at nodes 23, 7 and the substation 22. However, the circuit 7-23 was open in the scenario 2. This is understandable because the high-level DGs injections at nodes 23 and 7 will result in the voltage rise at node 8 when operating the circuit 7-23 in scenario 2.

The total cost of case 3 is \$121,100 (8.14%) higher than that of case 1. It shows that to determine the optimal connection point for the DG unit can effectively decrease the investment and operation cost by optimal power flow and further maximising the benefit of the DG applications. Note that the NPV and IRR in case 3 are close to that in case 1. This is understandable that the two cases have a roughly equal cost of purchasing electricity from the upstream power system as there is no curtailment of DG power in both cases.

iv. *Case 4:* The solution obtained in case 4 has an objective value of US\$1,422,100 and the case is solved in 76.8 min. In this case, it is assumed that the DGs operate with the leading power factor of 0.95 and ANM techniques are not included in this case. The solution in period 1 has the same topology as that in case 1, except the selected conductor types and the sizing of SVGs and VRs. In period 2, a type 1 VR was installed at the circuit 21-1 while substation 21 was upgraded with a capacity of by 12 MWA. Meanwhile, an SVG with a capacity of 50 kVAR was installed at node 14 to absorb the surplus of the reactive power brought by the DG therein. The SVG at node 21 was increased to the capacity of 1200 kVAR. In period 3, the SVG at substation 21 was reinforced by a capacity of 300 kVAR. In the period 3, node 10 was transferred to the substation 22 by opening circuit 3-23 in the scenario 1 while in the scenario 2 the load at node 3 was also supplied by substation 22 with circuit 3-2 open. This is mainly because in the scenario 2 the DGs with high-level output power at nodes 23 and 7 are capable of meeting demands at nodes 3, 10 and 11 so as to avoid the potential voltage rise resulting from the surplus of the reactive power from substation 21.

The total cost of case 4 is \$55,000 (3.87%) higher than that of case 1. It is mainly because additional capacities of SVGs and VRs would be invested in case 4 to absorb the surplus of reactive power due to the prohibition of ANM. As for NPV and IRR, there is little difference between cases 1 and 4. This is mainly because that there is no DG curtailment and the cost of purchasing electricity from the upstream power system are almost the same in both of these cases.

v. *Case 5:* The solution obtained in case 5 has an objective value of US\$ 1,426,900 and the case is solved in 38.4 min. In this case, the SVG is excluded from the alternative options. The system topologies in periods 1 and 2 are the same as those in case 1, except the size and sitting of VRs. Two type 1 VRs were, respectively, allocated to circuits 22-8 and 21-2 in period 1, while one VR was installed at circuit 21-1 in period 2. In the operating stage, the circuits 1-14 and 7-23 were open in the scenario 1 and the circuits 14-18 and 22-8 were open in the scenario 2 to keep open-loop operation for the distribution network.

The total cost of case 5 is \$59,800 (4.2%) higher than that of case 1. As shown in Table 5, the investment in case 5 is significantly higher than that in case 1. This is mainly because the SVG with a high degree of flexibility as the alternative option in case 1 contributes to the investment cost reduction compared with the VR in case 5. Note that the NPV and IRR in case 5 are the lowest among the five cases. This is reasonable because that the DG curtailment results in a comparatively high cost of purchasing electricity from the upstream power system.

4.3 Accuracy of the linearisation of (19)

In order to demonstrate the accuracy of the linearisation to the power flow equations after attaining the optimal solution, we present the voltage magnitude difference between our results and those of the Newton-Raphson method. A comparison is also made between our method and that of the lossless DC power flow in [4]. Fig. 6 depicts the results where the differences obtain based on our method are much smaller. The results demonstrate that our linearisation technique can lead to a higher accuracy for the expansion planning. Besides, the model proposed in this paper is solved in 50.1 min while it only takes 14.2 min when employing the lossless DC power flow. Although the DC power flow model has high solution speed, our model is still more preferable considering its higher level of accuracy and the long-term property of DNP.

5 Conclusions and future work

A multistage and multi-scenario planning model is presented for ADN, with investment decision-making and operation strategies co-optimised. The proposed model optimises the following alternatives comprehensively: upgrading capacities of substations, reinforcing and/or constructing the cable circuit, allocating VRs and/or SVGs, and choosing connection points for DGs. The operation strategy for each scenario is determined, wherein the active management of DGs, as well as the optimal ADN topology, is also produced. A MIQCP model is derived to guarantee the convergence to the optimality with the use of an off-the-shell solver. Case studies demonstrate that considering the multiple alternatives in the DNP model offers the most appropriate set of investment decisions and operation strategies to be implemented at a minimum cost. The disadvantages of our method and thus part of our future work comprise two aspects:

i. The uncertainties, e.g. the load consumption and power outputs of renewable DG units, play an important role in the DNP model. In our model, we used two typical scenarios to simulate the load and DGs' generation profile. In our future work, the uncertainties will be better modelled and simulated through interval-number methods or probabilistic methods to achieve a more applicable and practical planning scheme.

Table 4 Comparison of different cases

	Case1	Case2	Case3	Case4	Case5
Conditions					
DNR	✓	✗	✓	✓	✓
DG connection point	✓	✓	✗	✓	✓
Alternative options					
ANM	✓	✓	✓	✗	✓
SVG	✓	✓	✓	✓	✗
Number					
integer variables	1206	756	1188	1206	1134
continuous variables	6402	6375	6390	6366	6258
constraints	10,849	10,399	10,819	10,522	10,417
solution time, min	50.1	40.3	66.7	76.8	38.4

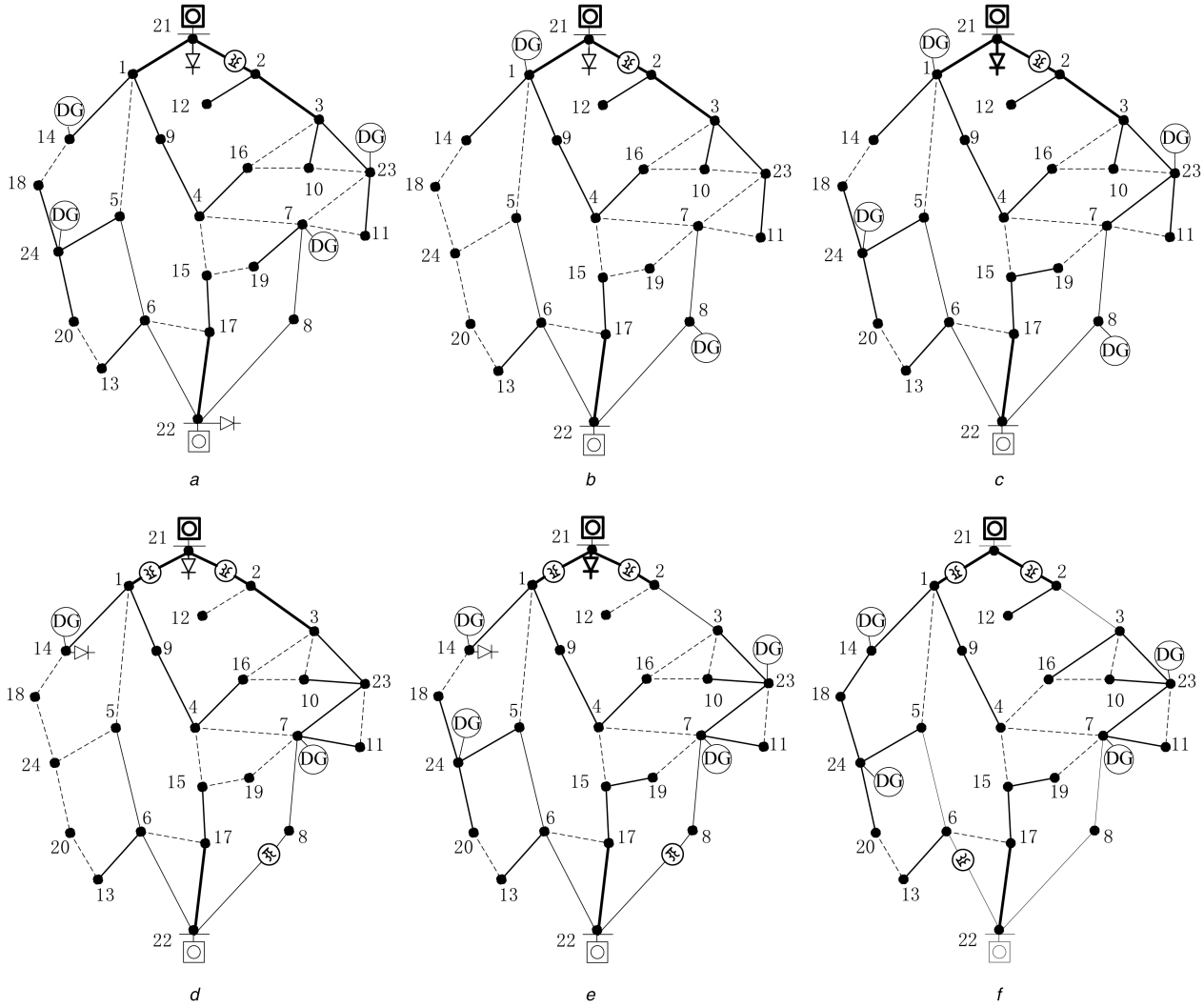

Fig. 5 *Topologies for cases 2–5*
(a) Case 2 period 3, ***(b)*** Case 3 period 2, ***(c)*** Case 3 period 3, ***(d)*** Case 4 period 2, ***(e)*** Case 4 period 3, ***(f)*** Case 5 period 3

Table 5 Economic analysis for five cases

Case		Case 1	Case 2	Case 3	Case 4	Case 5
cost, $10^3$$	investment	1326.6	1399.9	1441.5	1382.8	1373.5
	loss	39.3	40.2	46.7	39.3	38.1
	curtailment	1.2	0	0	0	15.3
	total	1367.1	1440.1	1488.2	1422.1	1426.9
NPV, $10^3$$		658.8	648.2	636.1	624.1	613.6
IRR, %		2.50	2.49	2.45	2.47	2.44

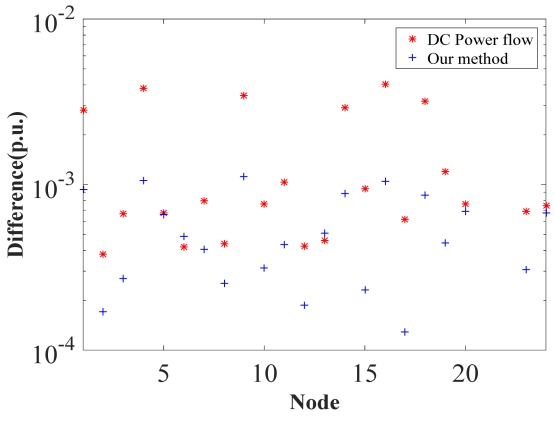

Fig. 6 *Accuracy of the linear power flow*

ii. As a variety of alternatives are incorporated into the proposed multistage DNP model, the complexity of the optimisation problem together with the consequent solution time will increase greatly, which is also validated by the case studies. Thus, it is necessary to decompose the solution method into several phases whereby the dimensions of the problem and the number of variables, especially that of integer variables, could be reduced to speed up the solving of DNP model.

6 Acknowledgments

This work was jointly supported by the National Natural Science Foundation of China (grant no. 51477151) and Postdoctoral Innovation Talent Support Program of China (grant no. BX201700211).

7 References

[1] Kothari, D.P., Nagrath, I.J.: '*Modern power system analysis*' (Tata McGraw-Hill, New York, 2011)

[2] Tabares, A., Franco, J., Lavorato, M.*, et al.*: 'Multistage long-term expansion planning of electrical distribution systems considering multiple alternatives', *IEEE Trans. Power Syst.*, 2016, **31**, (3), pp. 1900–1914

[3] Mohtashami, S., Pudjianto, D., Strbac, G.: 'Strategic distribution network planning with smart grid technologies', *IEEE Trans. Smart Grid*, 2017, **8**, (6), pp. 2656–2664

[4] Shen, X., Shahidehpour, M., Han, Y.*, et al.*: 'Multi-stage planning of active distribution networks considering the co-optimization of operation strategies', *IEEE Trans. Smart Grid*, 2018, **9**, (2), pp. 1425–1433

[5] Asensio, M., Munoz-Delgado, G., Contreras, J.: 'A bi-level approach to distribution network and renewable energy expansion planning considering demand', *IEEE Trans. Power Syst.*, 2017, **32**, (6), pp. 4298–4309

[6] Mansor, N., Levi, V.: 'Integrated planning of distribution networks considering utility planning concepts', *IEEE Trans. Power Syst.*, 2017, **32**, (6), pp. 4656–4672

[7] Parada, V., Ferland, J., Arias, M.*, et al.*: 'Optimization of electrical distribution feeders using simulated annealing', *IEEE Trans. Power Deliv.*, 2014, **19**, (2), pp. 1135–1141

[8] Zhao, C., Li, J., Zhang, Y.*, et al.*: 'Optimal location planning of renewable distributed generation units in distribution networks: an analytical approach', *IEEE Trans. Power Syst.*, 2018, **33**, (3), pp. 2742–2753

[9] Koutsoukis, N., Georgilakis, P., Hatziargyriou, N.: 'Multistage coordinated planning of active distribution networks', *IEEE Trans. Power Syst.*, 2018, **33**, (1), pp. 32–44

[10] Zhang, X., Che, L., Shahidehpour, M.*, et al.*: 'Reliability-based optimal planning of electricity and natural gas interconnection for multiple energy hubs', *IEEE Trans. Smart Grid*, 2017, **8**, (4), pp. 1658–1667

[11] Munoz-Delgado, G., Contreras, J., Arroyo, J.: 'Multistage generation and network expansion planning in distribution systems considering uncertainty and reliability', *IEEE Trans. Power Syst.*, 2016, **31**, (5), pp. 3715–3728

[12] Delgado, G., Contreras, J., Arriyo, J.: 'Distribution network expansion planning with an explicit formulation for reliability assessment', *IEEE Trans. Power Syst.*, 2018, **33**, (3), pp. 2583–2596

[13] Alkaabi, S., Khadkikar, V., Zeineldin, H.: 'Incorporating PV inverter control schemes for planning active distribution networks', *IEEE Trans. Sustain. Energy*, 2015, **6**, (4), pp. 1224–1233

[14] Xing, H., Cheng, H., Zeng, P.: 'Active distribution network expansion planning integrating dispersed energy storage systems', *IET Gener. Transm. Distrib.*, 2016, **10**, (5), pp. 638–644

[15] Dzamarija, M., Keane, A.: 'Firm and non-firm wind generation planning considering distribution network sterilization', *IEEE Trans. Smart Grid*, 2013, **4**, (4), pp. 2162–2173

[16] Khodaei, A., Shahidehpour, M., Wu, L.*, et al.*: 'Coordination of short-term operation constraints in multi-area expansion planning', *IEEE Trans. Power Syst.*, 2012, **27**, (4), pp. 2242–2250

[17] Cortes, C., Contreras, S., Shahidehpour, M.: 'Microgrid topology planning for enhancing the reliability of active distribution networks', *IEEE Trans. Smart Grid*, 2017, doi: 10.1109/TSG.2017.2709699

[18] Dias, F.M., Canizes, B., Knodr, H.: 'Distribution networks planning using decomposition optimization technique', *IET Gener. Transm. Distrib.*, 2015, **9**, (12), pp. 1409–1420

[19] Che, L., Zhang, X., Shahidehpour, M.*, et al.*: 'Optimal interconnection planning of community microgrids with renewable energy sources', *IEEE Trans. Smart Grid*, 2017, **8**, (3), pp. 1054–1063

[20] Shu, J., Wu, L., Li, Z.*, et al.*: 'A new method for spatial power network planning in complicated environments', *IEEE Trans. Power Syst.*, 2012, **27**, (1), pp. 381–389

[21] Taylor, J.A., Hover, F.S.: 'Convex models of distribution system reconfiguration', *IEEE Trans. Power Syst.*, 2012, **27**, (3), pp. 1407–1413

[22] El-Zonkoly, A.M.: 'Multistage expansion planning for distribution networks including unit commitment', *IET Gener. Transm. Distrib.*, 2013, **7**, (7), pp. 766–778

[23] Li, N., Chen, L., Low, S.: 'Exact convex relaxation of OPF for radial networks using branch flow model'. 2012 IEEE Third Int. Conf. SmartGridComm, Tainan, Taiwan, 2012, pp. 1–7

[24] Rahimiyan, M., Baringo, L., Conejo, A.J.: 'Energy management of a cluster of interconnected price-responsive demands', *IEEE Trans. Power Syst.*, 2014, **29**, (2), pp. 645–655

[25] Nguyen, D.T., Le, L.B.: 'Risk-constrained profit maximization for microgrid aggregators with demand response', *IEEE Trans. Smart Grid*, 2015, **6**, (1), pp. 135–146

[26] Lavorato, M., Franco, J.F., Rider, M.J.*, et al.*: 'Imposing radiality constraints in distribution system optimization problems', *IEEE Trans. Power Syst.*, 2012, **27**, (1), pp. 172–180

[27] Franco, F., Rider, M.J., Lavorato, M.*, et al.*: 'A mixed-integer LP model for the reconfiguration of radial electric distribution systems considering distributed generation', *Electr. Power Syst. Res.*, 2013, **97**, (97), pp. 51–60

[28] Achterberg, T.: 'SCIP: solving constraints integer programs', *Program. Comput.*, 2009, **1**, (1), pp. 1–41